Supplementary Information

Enhanced interfacial charge separation via $MnIn_2S_4/Zn_2TiO_4$ heterojunction for light-induced fuel production

Plassidius J. Chengula[a], Junying Zhang[b], Hazina Charles[a], Ji Yeon Seo[a], Xiaofang Jia*[c], Caroline Sunyong Lee*[a]

[a] Department of Materials and Chemical Engineering, Hanyang University, Gyeonggi-do 426-791, Korea. Email: sunyonglee@hanyang.ac.kr

[b] School of Physics, Beihang University, Beijing 100191, China. Email: zjy@buaa.edu.cn

[c] School of Physical Science and Technology, Inner Mongolia University, Hohhot 010021, China. Email: jiaxiaofang@imu.edu.cn

* Co-Corresponding authors:

Email: sunyonglee@hanyang.ac.kr; jiaxiaofang@imu.edu.cn

S1. Photoelectrochemical measurements

Photoelectrochemical (PEC) measurements including photocurrent response, Mott–Schottky analysis, and electrochemical impedance spectroscopy were performed using a VersaSTAT 4 electrochemical workstation (Princeton Applied Research, USA) in a standard three-electrode configuration. The setup included a photocatalyst-modified working electrode, a platinum wire counter electrode, and an Ag/AgCl reference electrode with a 0.5 M Na_2SO_4 aqueous solution used as the electrolyte. All measurements were conducted under an applied bias of 0.2 V (vs. Ag/AgCl).

The working electrodes were prepared by depositing the photocatalyst onto fluorine-doped tin oxide (FTO) glass substrates with an active area of 2 × 2 cm^2. In brief, MIS, ZTO, and MIS/ZTO powders were dispersed separately in isopropyl alcohol (IPA) by ultrasonication to form suspensions (0.2 g catalyst in 2 mL IPA). An aliquot of each suspension was spin-coated onto cleaned FTO substrates at 2500 rpm for 60 s. The resulting films were dried at 60 °C for 2 h and annealed in argon atmosphere at 200 °C for an additional 2 h for removing the residual solvent and improving film adhesion. All PEC measurements were conducted under UV–vis illumination using a 300 W xenon lamp as the light source.

S2. Photocatalytic CO_2 reduction

The CO_2 photoreduction tests were performed in a custom-designed quartz reactor with a total volume of 250 mL using an immobilized thin-film catalyst configuration. Initially, 200 mg of MIS, ZTO, or MIS/ZTO powder was dispersed in 2 mL of isopropanol (IPA) through ultrasonication, followed by magnetic stirring for 5 days to achieve uniform suspension. This dispersion was then spin-coated onto a pre-cleaned and pre-weighed FTO substrate at 2500 rpm for 60 s. After drying at 200 °C for 2 h under argon atmosphere, the coated substrate was

weighed again, so that the deposited catalyst mass was determined by subtracting the mass of the bare FTO, resulting in an effective loading of 2.0 mg. For each experimental run, the FTO-supported film containing 2.0 mg of catalyst was placed in a reaction mixture composed of 125 mL of distilled water and 25 mL of triethanolamine (TEOA), which served as a sacrificial hole scavenger. Before initiating the reaction, the reactor was sealed with a septum and positioned above the aqueous solution. Subsequently, the system was evacuated and filled with high-purity CO_2 (99.99%) from a gas cylinder, maintaining a pressure of ~2 bar. The reactor was purged continuously with CO_2 for 2 h to ensure the complete removal of residual air. Gaseous products generated during the photoreduction process were analyzed using a gas chromatograph (6500GC, YL Instruments, Korea) equipped with a fused-silica capillary column, pulsed discharge detector, and flame ionization detector, with helium employed as the carrier gas. Photocatalytic reactions were driven by UV–vis irradiation from a 300 W Xe arc lamp (Model 66984; Newport, USA).

To assess cycling stability, the catalyst film was retrieved after each reaction cycle and rinsed thoroughly three times with deionized water to remove any residual reactants or products. Then, the film was dried in an oven at 60 °C overnight. Before starting a subsequent cycle, the reactor was purged with high-purity argon for 20 min to eliminate any remaining gaseous species and avoid cross-contamination between runs.

S3. Apparent quantum efficiency

The wavelength-dependent apparent quantum yield (AQY) of CO_2 photoreduction on 0.4-MIS/ZTO is calculated using different monochromatic light sources. The AQY is defined as the ratio of the total number of electrons participating in reduction reactions to the total number of incident photons. Therefore, AQY can be calculated by:

$$AQY(\%) = \frac{6 \times Y_{CH3OH}}{The\ number\ of\ incident\ photons} \times 100\%\ (1)$$

where Y_{CH3OH} represent the yields CH_3OH. The number of incident photons is calculated by:

$$The\ number\ of\ incident\ photons = \frac{PS\lambda t}{N_A hc}\ (2)$$

where the irradiation area (S) is 12.57 cm^2, t is the irradiation time (25200 s), λ is the irradiation wavelength (350, 420 and 500 nm), N_A is the Avogadro constant (6.022×10^{23} mol^{-1}), h is the Planck constant (6.63×10^{-34} J·s) and c is the speed of the light (3×10^8 m s^{-1}). The average light intensity (P) was measured to be 0.19 mW cm^{-2} for 350 nm, 0.30 mW cm^{-2} for 420 nm and 0.48 mW cm^{-2} for 500 nm. The corresponding methanol yield was measured to be 7.83 μmol for 350 nm, 6.15 μmol for 420 nm and 3.03 μmol for 500 nm.

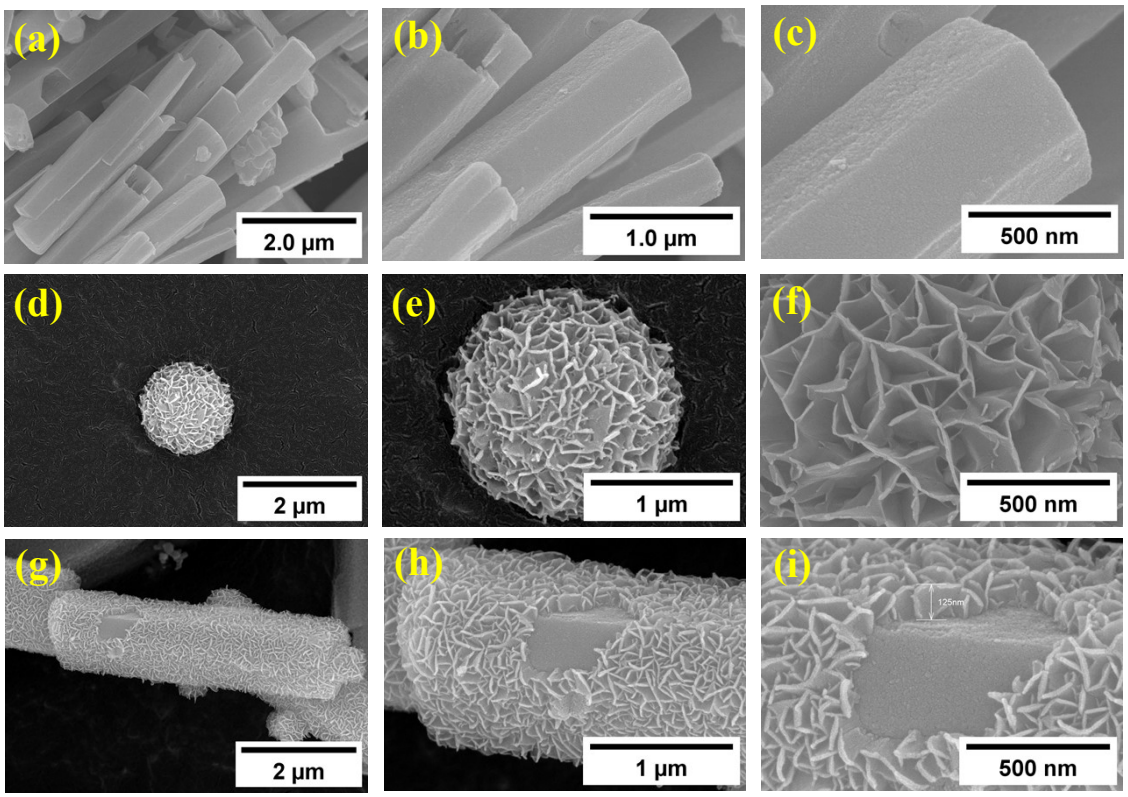

Fig. S1. FE-SEM images of (a–c) Zn_2TiO_4, (d–f) $MnIn_2S_4$, and (g–i) $MnIn_2S_4/Zn_2TiO_4$ heterostructures.

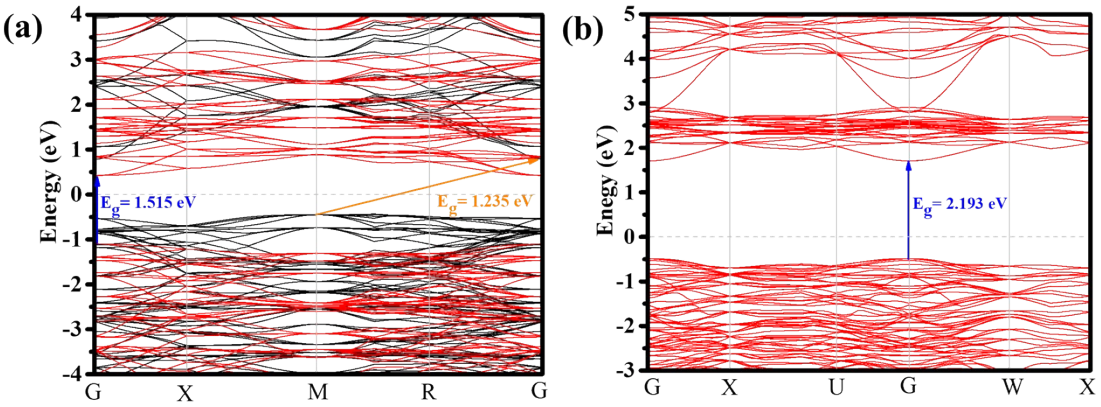

Fig. S2. Band structure of (a) $MnIn_2S_4$ (b) Zn_2TiO_4.

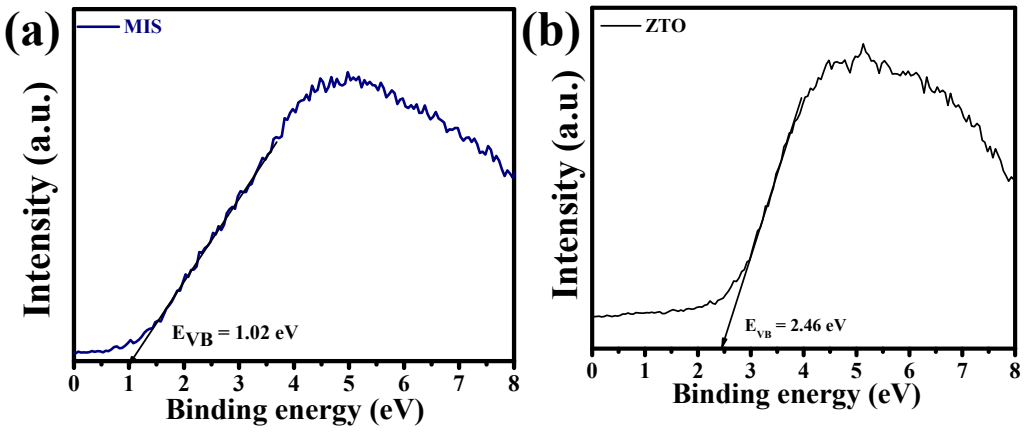

Fig. S3. Valence band energy maximum of (a) MIS (b) ZTO determined using XPS valence band spectra.

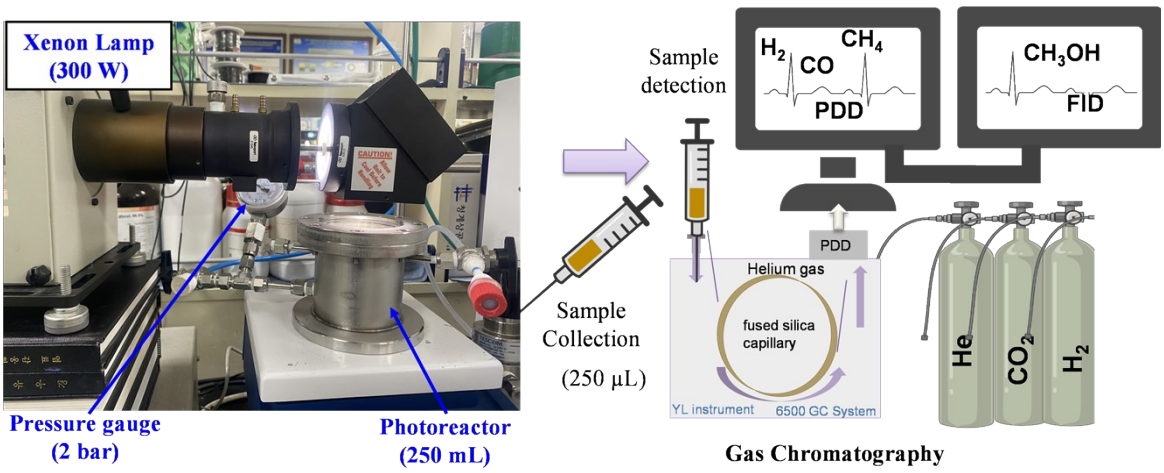

Fig. S4. CO_2 photoreactor setup.

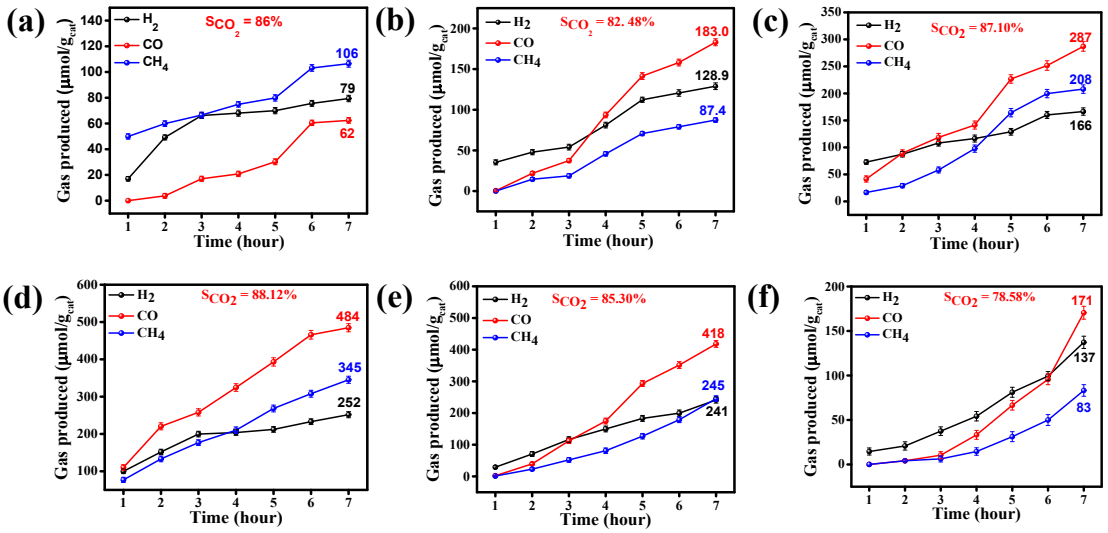

Fig. S5. CO_2 photoreduction activities of (a) Zn_2TiO_4, (b) 0.1$MnIn_2S_4/Zn_2TiO_4$ (c) 0.2 $MnIn_2S_4/Zn_2TiO_4$ (d) 0.4 $MnIn_2S_4/Zn_2TiO_4$ (e) 0.6 $MnIn_2S_4/Zn_2TiO_4$ (f) $MnIn_2S_4$ for H_2, CO and CH_4 generation.

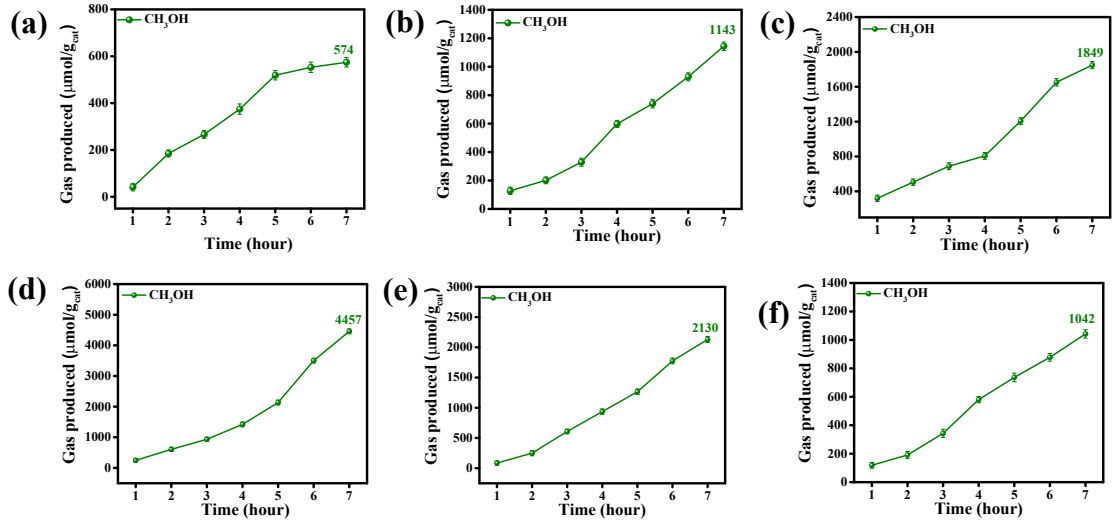

Fig. S6. CO_2 photoreduction activities of (a) Zn_2TiO_4, (b) 0.1$MnIn_2S_4/Zn_2TiO_4$ (c) 0.2 $MnIn_2S_4/Zn_2TiO_4$ (d) 0.4 $MnIn_2S_4/Zn_2TiO_4$ (e) 0.6 $MnIn_2S4/Zn_2TiO_4$ (f) $MnIn_2S_4$ for CH_3OH production.

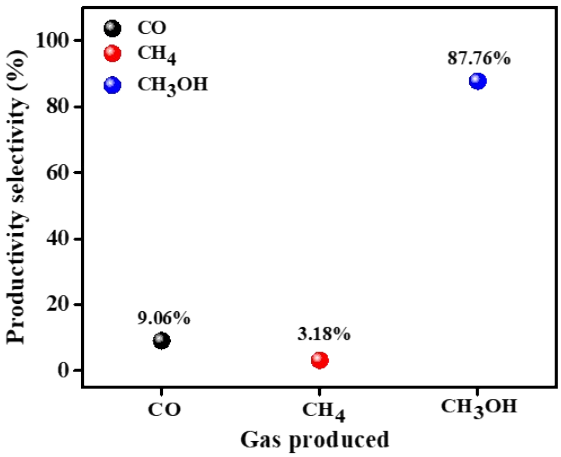

Fig. S7. Product selectivity based on overall yield of 0.4-MIS/ZTO

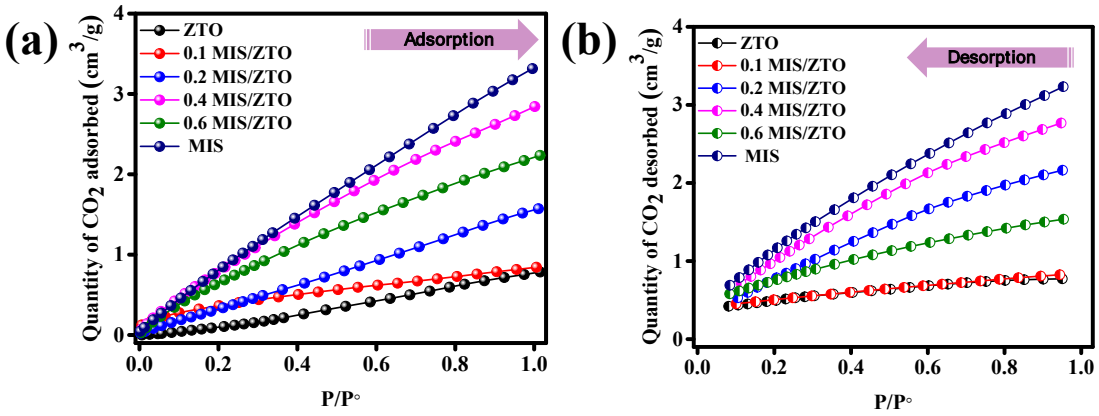

Fig. S8. CO_2 adsorption (a) and desorption (b) of ZTO, MIS, and MIS/ZTO heterostructures

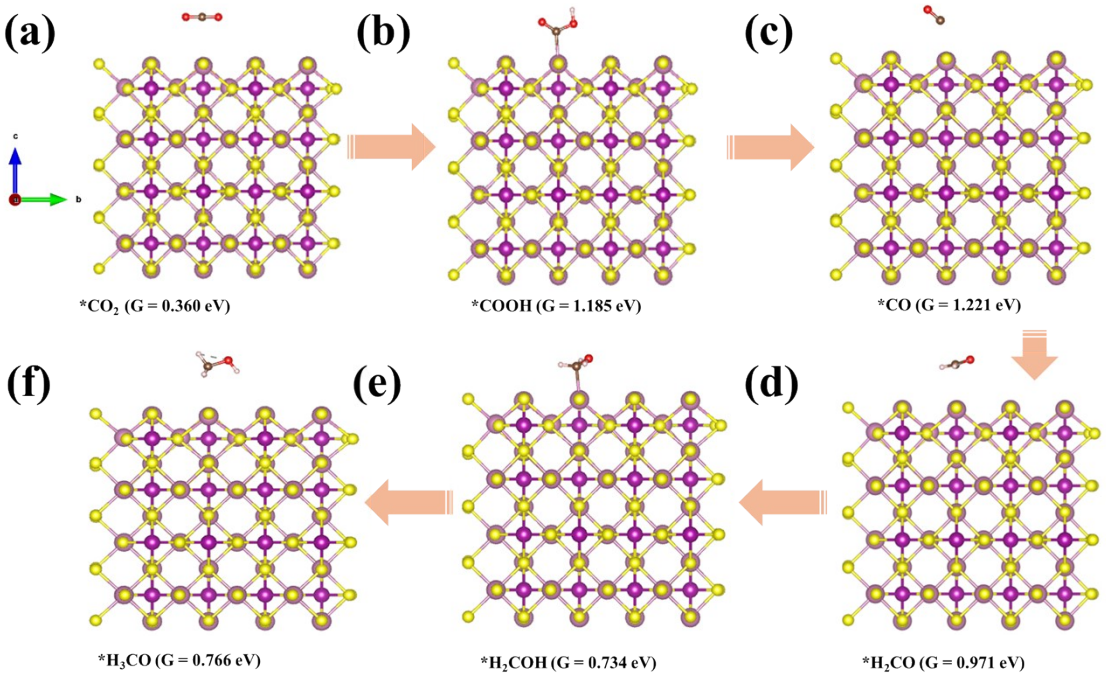

Fig. S9. Optimized adsorption geometries structures of intermediates on reaction sites of the surface of MIS.

Table S1. Total carbon balance of 0.4-MIS/ZTO

Product	**Product amount (umol)**	**Carbon per molecule**	**Carbon (umol)**
CO	0.97	1	0.97
CH_4	0.69	1	0.69
CH_3OH	8.91	1	8.91
Total	10.57		10.57

Table S2. Comparison of the reaction conditions and performances with titanates-based catalysts for photocatalytic CO_2 reduction.

Photocatalyst	**Light source**	**Reaction medium**	**Product**	**Yield ($\mu molg^{-1} h^{-1}$)**	**Ref**
Al-doped $SrTiO_3$	400 W high-pressure	0.1 M aq. $NaHCO_3$ solution	CO	64.6	1

$CaTiO_3$	Hg lamp ($\lambda > 300$ nm) 100 W high-pressure Hg lamp ($\lambda = 254$ nm)	0.5 M aq. $NaHCO_3$ solution	CO	24.4	2
$CaTiO_3$	400 W high-pressure Hg lamp	1.0 M aq. $NaHCO_3$ solution	CO	14.36	3
$SrTiO_3$	300 W UV-enhanced Xe-lamp ($\lambda > 420$ nm)	Aqueous H_2O	CO CH_4	0.349 0.231	4
V_O-$SrTi_{0.8}Mn_{0.2}O_3$	Xe lamp (0.2 W cm^{-2})	H_2O vapor	CH_4	6.07	5
Pt/$SrTiO_3$	300 W Xe-lamp (320 < λ < 780 nm)	Aqueous H_2O	CO CH_4	4.1 26.7	6
Bi-doped $SrTiO_3$	300 W UV-enhanced Xe-lamp, ($\lambda > 420$ nm)	Aqueous H_2O	CO CH_4	5.58 0.36	7
Defective $Bi_2Ti_2O_7/TiO_2$	300 W Xe lamp	H_2O vapor	CH_4	6.8	8
CaTiO3	UV-lamp (6 W cm^{-2})	H_2O	CH_4	2.43	9
Ti-rich $SrTiO_3$	Xe lamp (0.19 W cm^{-2})	H_2O vapor	CO	4.4	10
$BaTiO_3$	400 W high-pressure Hg lamp	1.0 M aq. $NaHCO_3$ solution	CO	3.04	3
V_O-$SrTiO_3$/Ag	Xe lamp ($\lambda > 420$ nm, 0.2 W cm^{-2})	H_2O +TEOA	CO	2.0	11
20% $FeTiO_3/TiO_2$	500 W, Xe lamp (λ < 300 nm)	0.08 M aq. $NaHCO_3$ solution	CH_3OH:	0.46	12

$NiTiO_3$ NFs	300 W Xe-lamp (320 < λ < 780 nm)	H2O+TEOA	CO	57.833	[13]
			CH_4	24.33	
$NiTiO_3$/g-C_3N_4	A 300 W Xe lamp. (λ > 420 nm)	H_2O	CH_3OH	13.74	[14]
Ga-doped $NiTiO_3$	90 W LED (visible range)	0.1 M aq. $NaHCO_3$ solution	CH_3OH	84.45	[15]
			CH_4	21.35	
			CO	16.28	
Bi_2Te_3/$SrTiO_3$	300 W Xe lamp	H_2O vapor	H_2	27.86	[16]
			CO	28.0	
			CH_4	1.4	
Carbon QD/TiO_2–$SrTiO_3$	300 W Xe lamp	H_2O	CO	54.9	[17]
			CH_4	35.9	
Cu species/$SrTiO_3$	300 W Xe lamp	H_2O	CH_3OH	8.08	[18]
Oxygen vacancy + Cu/$SrTiO_3$	300 W Xe lamp	H_2O	CH_3OH	5.75	[19]
$ZnIn_2S_4$/$SrTiO_3$In$(OH)_3$	300 W Xe lamp (λ > 420 nm)	aqueous H_2O	CO	39.4	[20]
$Bi_2O_2CO_3$/$SrTiO_3$	300 W Xe lamp	Aqueous H_2O	CH_4	35.62	[21]
TiO_2 NPs/$SrTiO_3$	300 W Xe lamp	Aqueous H_2O	CO	11.35	[22]
			CH_4	164.55	
Bi_2SiO_5/$SrTiO_3$	300 W Xe lamp	Aqueous H_2O	CO	15.89	[23]
			CH_4	10.60	
$CsPbBr_3$/$SrTiO_3$	300 W Xe lamp (λ > 420 nm)	Aqueous H_2O	CO	1.64	[24]
			CO	120.2	
Ag/ $SrTiO_3$	300 W Xe lamp	MeCN+ H_2O	CH_4	4.21	[25]

			CO	20.06	
			H_2	5.75	
$ZnFe_2O_4/SrTiO_3$	300 W Xe lamp	Aqueous H_2O	CH_4	2.51	[26]
	($\lambda > 420$ nm)		CO	8.24	
Cr-doped $SrTiO_3$	300 W Xe lamp	Aqueous H_2O	CH_4	0.88	[27]
	($\lambda \approx 420$ nm)				
Hydrogenated $SrTiO_3$	Ultraviolet lamp	Aqueous H_2O	C_2H_2	6.49	[28]
	($\lambda > 254$ nm)		CO	3.32	
			CH_4	1.96	
			CH_3OH	**636.71**	
$MnIn_2S_4$/ Zn_2TiO_4	**300 W Xe-lamp**	**H_2O**	**CH_4**	**49.28**	**This work**
	($320 < \lambda < 780$ nm)		**CO**	**69.14**	
			H_2	**36.00**	

References

1 S. Wang, K. Teramura, T. Hisatomi, K. Domen, H. Asakura, S. Hosokawa and T. Tanaka, *Chemical Science*, 2021, **12**, 4940–4948.

2 S. Wang, K. Teramura, T. Hisatomi, K. Domen, H. Asakura, S. Hosokawa and T. Tanaka, *ACS Sustainable Chemistry and Engineering*, 2021, **9**, 9327–9335.

3 T. Ishii, A. Anzai, A. Yamamoto and H. Yoshida, *Applied Catalysis B: Environmental*, 2020, **277**, 119192.

4 H. Zhou, J. Guo, P. Li, T. Fan, D. Zhang and J. Ye, *Scientific Reports*, 2013, **3**, 1–9.

5 H. Zhou, J. Guo, P. Li, T. Fan, D. Zhang and J. Ye, *Scientific Reports*, 2013, **3**, 1667.

6 X. Wu, C. Wang, Y. Wei, J. Xiong, Y. Zhao, Z. Zhao, J. Liu and J. Li, *Journal of Catalysis*, 2019, **377**, 309–321.

7 L. Pan, H. Mei, G. Zhu, S. Li, X. Xie, S. Gong, H. Liu, Z. Jin, J. Gao, L. Cheng and L. Zhang, *Journal of Colloid and Interface Science*, 2022, **611**, 137–148.

8 D. Zhang, Y. jie Sun, X. Tian, X. T. Liu, X. jing Wang, J. Zhao, Y. pei Li and F. tang Li, *Journal of Colloid and Interface Science*, 2022, **606**, 1477–1487.

9 B. S. Kwak and M. Kang, *Applied Surface Science*, 2015, **337**, 138–144.

10 C. Luo, J. Zhao, Y. Li, W. Zhao, Y. Zeng and C. Wang, *Applied Surface Science*, 2018, **447**, 627–635.

11 K. Shao, Y. Wang, M. Iqbal, L. Lin, K. Wang, X. Zhang, M. He and T. He, *Applied Surface Science*, 2018, **434**, 717–724.

12 Q. D. Truong, J.-Y. Liu, C.-C. Chung and Y.-C. Ling, *Catalysis Communications*, 2012,

19, 85–89.

13 H. Khan, H. Charles, P. J. Chengula, P. J. Yoo, K.-H. Kim and C. S. Lee, *Ceramics International*, 2024, **50**, 13832–13840.

14 H. Guo, S. Wan, Y. Wang, W. Ma, Q. Zhong and J. Ding, *Chemical Engineering Journal*, 2021, **412**, 128646.

15 A. Kumar Sahu, S. Yadav, D. Banerjee, T. E. Rufford and S. Upadhyayula, *ACS Applied Materials & Interfaces*, 2024, **16**, 7057–7069.

16 S. Xing, G. Ba, C. Qin, H. Hu, J. Ye and D. Wang, *Catalysts*, 2025, **15**, 229.

17 Q. Wang, Y. Yuan, C. Li, Z. Zhang, C. Xia, W. Pan, L. Liu and R. Guo, *Renewable Energy*, 2024, **231**, 120997.

18 X. Guo, C. Qiu, Z. Zhang, J. Zhang, L. Wang, J. Ding, J. Zhang, H. Wan and G. Guan, *Journal of Environmental Chemical Engineering*, 2024, **12**, 111990.

19 J. Zhang, C. Qiu, L. Wang, R. Chen, J. Ding, J. Zhang, H. Wan and G. Guan, *Ceramics International*, 2024, **50**, 39374–39381.

20 B. Ding, K. Zuo, L. Zhang, S. Liu, S. Zheng, L. Mao and J. Zhang, *Journal of Environmental Chemical Engineering*, 2024, **12**, 114594.

21 Z. Li, J. Xu, Y. An, S. Mj Zubairu, W. Zhang, L. Zhu, J. Li, X. Xie and G. Zhu, *Separation and Purification Technology*, 2023, **311**, 123323.

22 J. Ge, Y. He, X. Yue, Q. Chen, Q. Zhang, R. Liu, D. Wang, A. Wu and C. Tian, *Chemical Engineering Journal*, 2026, **531**, 174185.

23 T. Han, Y. Guo, M. A. Mushtaq and Y. Jia, *Journal of Environmental Chemical*

Engineering, 2025, **13**, 117604.

24 S. Yuan, K. Su, Y. Feng, M. Zhang and T. Lu, *Chinese Chemical Letters*, 2023, **34**, 107682.

25 S. Wan, M. Chen, M. Ou and Q. Zhong, *Journal of CO2 Utilization*, 2019, **33**, 357–364.

26 Y. Jia, H. Han, Y. Luo, Q. Wang, B. Wha Lee and C. Liu, *Separation and Purification Technology*, 2023, **306**, 122667.

27 Y. Bi, M. F. Ehsan, Y. Huang, J. Jin and T. He, *Journal of CO2 Utilization*, 2015, **12**, 43–48.

28 H. Xu, Z. Wang, H. Liao, D. Li, J. Shen, J. Long, W. Dai, X. Wang and Z. Zhang, *Applied Catalysis B: Environmental*, 2023, **336**, 122935.